5.3

ANALYSIS OF NUMERICALLY SIMULATED GRAVITY WAVES GENERATED BY CONVECTION

Zachary A. Eitzen[1] and David A. Randall
Colorado State University, Ft. Collins, Colorado

1. INTRODUCTION

In this abstract, we will study a simulation of convection, and the resulting generation of gravity waves that propagate into the surrounding environment. Vertically propagating gravity waves carry a momentum flux that may alter the mean winds at altitudes above the convection by well-known processes (Eliassen and Palm, 1960). Convectively generated gravity waves may carry a momentum flux of similar magnitude to that of orographically-generated waves (Fritts and Nastrom, 1992), which have long been acknowledged as important to the flow for altitudes at and above the upper troposphere (Bretherton, 1969). Researchers such as Dunkerton (1997) have identified vertically propagating convectively generated gravity waves as being an important cause of the quasi-biennial oscillation (Baldwin et al., 2001).

2. SIMULATION

The numerical simulation that will be analyzed here was a two-dimensional simulation performed using the Advanced Regional Prediction System (ARPS - see Xue et al. 2000). ARPS is a compressible model with full moist physics.The domain used in the simulation was 900 km wide, and 48 km high (the upper 16 km of which was a sponge layer). Horizontal grid spacing was 1 km, and vertical grid spacing was 250 m. The horizontal boundaries were periodic, and the domain moved with the storm at 16 m s^{-1} relative to the ground. The model was initialized with horizontally homogenous conditions based upon a sounding given by Weisman and Klemp (1982), which is an analytical sounding based on observed midlatitude squall lines that has been used in other vertically-propagating gravity wave studies (Fovell et al. 1992, Alexander et al. 1995). The initial wind profile that was used contains most of its 15 m s^{-1} of shear in the lowest 5 km of the atmosphere, and no shear in the stratosphere.

The simulation generated vertically-propagating gravity waves of a wide variety of horizontal wavelengths that travel away from the storm, as seen in Fig. 1. The simulated displacement of the isentropes ranged up to several hundred meters at altitudes of approximately 20 km, as has been observed by Pfister et al. (1993). This figure is quite similar to Fig. 2 of Alexander et al. (1995).

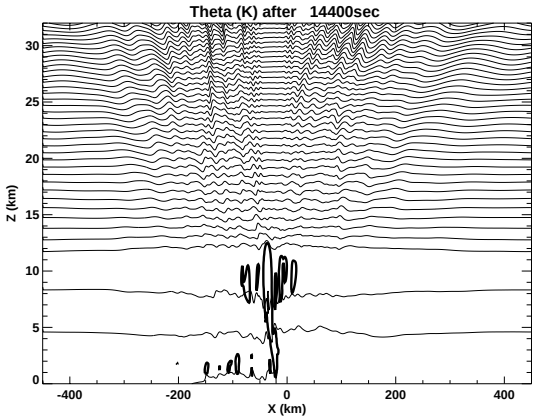

Fig. 1. The simulation after 4 hours. Thin lines represent isentropes (15 K interval), the thick line is the contour of 0.1 g/kg of cloud condensate.

3. TRAJECTORIES

In this section, we will examine the use of particle trajectories to qualitatively examine the behavior of air parcels in a numerical simulation of convection. Many physical fields produced by the numerical simulation were saved every 120 seconds into history files. The components of velocity from these history files were used to construct the background flow for the particles. The method used to advect the particles is the fourth-order Runge-Kutta scheme, similar to that used by Krueger et al. (1995).

In addition to calculating the position and speed of the particles, we can also interpolate the values of other scalar variables to the particles' positions. Once the trajectories are obtained, statistics can be calculated for the particles, some of

1. *Corresponding author address*: Zachary A. Eitzen, Department of Atmospheric Science, Colorado State University, Ft. Collins, CO 80521. e-mail: zach@atmos.colostate.edu

which can be combined in an attempt to isolate convective motions from non-convective motions (including gravity waves). One such statistic is a normalized mean vertical velocity, given by

$$\hat{w} = \frac{\overline{w}}{(\overline{w^2})^{1/2}} . \quad (1)$$

Here, the averages are temporal averages taken along each particle's path. This quantity should be near 1 for a particle that goes straight up, -1 for a particle that goes straight down, and 0 for particles with oscillatory or no vertical motion. The magnitude of a particle's displacement over the time period of the trajectory integration can be determined by calculating

$$\delta z = z_{max} - z_{min} . \quad (2)$$

Finally, if we also calculate the average cloud condensate (liquid water plus ice) along a particle's path $\overline{q_c}$, we can establish the following criteria for convective updraft motions:

$$\begin{aligned} \hat{w} &> 0 \quad , \\ \delta z &> 2000 \text{ m} \quad , \\ \overline{q_c} &> 10^{-1} \text{ g/kg} \quad . \end{aligned} \quad (3)$$

Particles were released at 1 km intervals in the horizontal and 0.25 km intervals in the vertical in the lower 13 km of the domain, starting at t = 4 h. The particles were released for 30 minutes, to obtain an optimal amount of separation between updraft and non-updraft particles. A scatter plot of the normalized vertical velocity versus displacement is shown in Fig. 2.

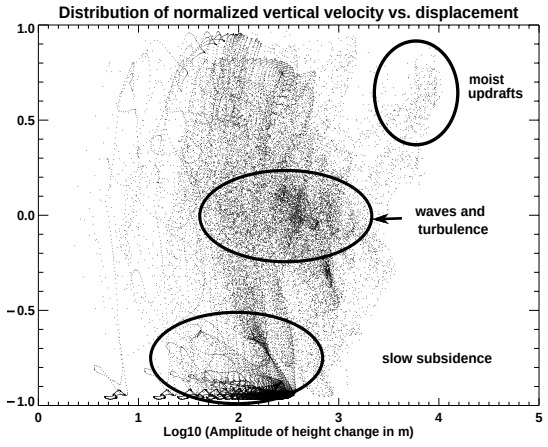

Fig. 2. Normalized vertical velocity versus $\log_{10}$ displacement in meters.

Physical interpretations can be made of several of the regions in the plot. The trajectories with the highest displacements also move up on average, and pass through regions with high concentrations of condensate (not shown) as well, indicating that these particles can be associated with moist convective updrafts. The many particles that have displacements of 50 - 500 m and a convective factor near -1 are affected by the slow subsidence outside of the storm. The particles with significant displacements and a convective factor near zero are undergoing wave or turbulent motions, oscillating about their initial position.

4. CLOUD MASKING

In addition to particle trajectory diagnosis, another technique for identifying cloudy and updraft particles is to apply criteria to the individual snapshots of the storm evolution. If the location of a data point has sufficient condensate ($\overline{q_c} > 10^{-1}$ g/kg) to be a cloudy particle, then that location is assigned a "cloud mask" value of 1. Otherwise, the cloud mask has a value of 0. The contribution of cloudy grid points to the covariance or variance of a quantity can then be calculated at each vertical level according to the sum,

$$(\overline{a'b'})_{\text{clouds}} = \frac{1}{nx} \sum_{i=1}^{nx} \text{CM}_i a_i' b_i' . \quad (4)$$

Here, CM_i is the value of the cloud mask at the *i*th location, a' and b' are the departures of the variables a and b from the horizontal mean. When (4) is a variance calculation, $a = b$. The criteria for updraft mask (UM) includes the condensate concentration, but also includes a vertical velocity threshold, i.e.,

$$\text{UM}_i = \begin{cases} 1 & \text{if } \overline{q_c} > 10^{-1} \text{ g/kg and } w > 1 \text{ m s}^{-1} ; \\ 0 & \text{otherwise.} \end{cases} \quad (5)$$

Note that updraft points are a subset of cloudy points according to the above criteria. These criteria are similar to those that obtained good separation between updraft points and non-updraft points in the trajectory analysis.

When the perturbation kinetic energy, defined by

$$\frac{1}{2}\rho_0 (\overline{u'u'} + \overline{w'w'}) \quad , \quad (6)$$

is vertically integrated throughout the troposphere, a measure of the amount of the average perturbation kinetic energy contained in a troposphere-deep 1 m^2 column is obtained.

The contribution of the cloudy and updraft points to the tropospheric integral of the vertical component of perturbation kinetic energy is shown in Fig. 3. The cloudy and updraft points account for a large fraction of the tropospheric kinetic energy, despite the fact that they cover a relatively small fraction of points (not shown). We see that the non-

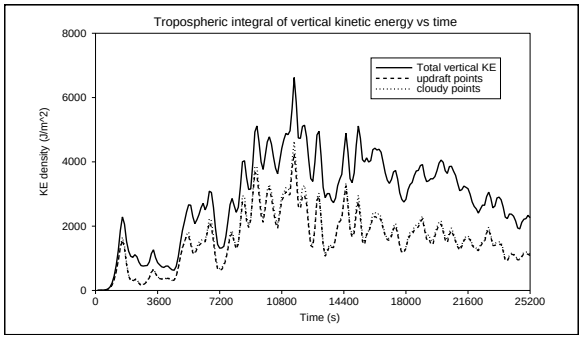

Fig. 3. Vertically integrated perturbation kinetic energy of the troposphere due to vertical motions versus time for all points, cloudy points, and updraft points.

updraft cloudy points do not contribute much to the total amount of $\overline{w'w'}$ in the troposphere in this simulation, despite the fact that there are similar numbers of updraft and non-updraft points within the set of cloudy points (not shown).

The contribution of the cloudy and updraft points to the tropospheric integral of the horizontal component of perturbation kinetic energy is shown in Fig. 4. Note that the magnitude of the horizontal component of kinetic energy is far higher than that of the vertical component. In addition, the non-

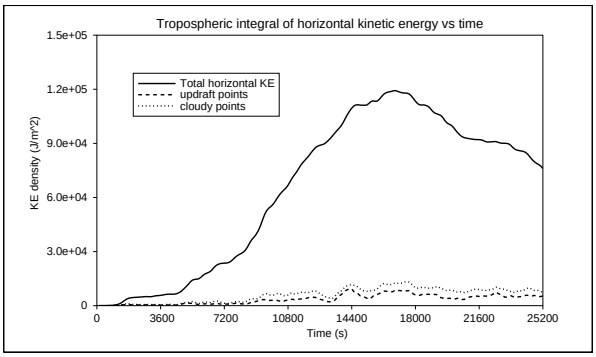

Fig. 4. Vertically integrated perturbation kinetic energy of the troposphere due to horizontal motions versus time for all points, cloudy points, and updraft points.

updraft points are clearly the dominant contributor to the total amount of $\overline{u'u'}$ within the troposphere. There is also far more separation between the contributions from the updraft and cloudy points in this field.

5. WAVES AS AN ENERGY SINK

The effect of convectively-forced vertically propagating gravity waves on the convection itself is not something that has received much attention in the literature. However, if one predicts a quantity that is associated with the kinetic energy of moist convection in a large-scale model (Randall and Pan, 1993), it would be useful to know how much energy is leaving the troposphere due to the waves. This wave energy flux $\overline{p'w'}$ can then be associated with the wave momentum flux using relationships similar to those of Eliassen and Palm (1960).

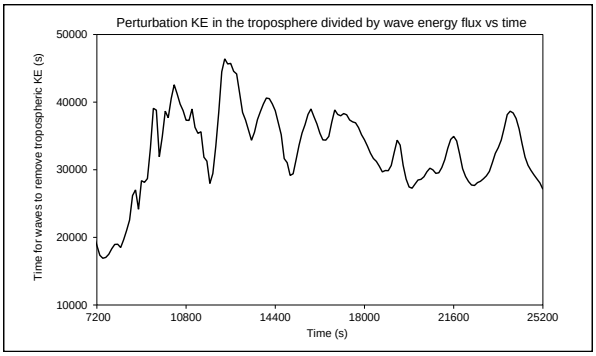

Fig. 5. Integrated perturbation kinetic energy of the troposphere divided by the wave energy flux at an altitude of 14000 m versus time.

In Fig. 5, we have calculated the value of a timescale for the removal of kinetic energy in the troposphere, defined by the integral of the energy defined in (6) divided by the wave energy flux at 14000 m, slightly above the model tropopause. We see that the in the mature stage of the storm (after t = 10800 s), this timescale appears to oscillate around a value of 35000 seconds, or approximately ten hours. Of course, this is only a single simulation, so any general conclusions regarding the magnitude of this timescale cannot yet be made.

6. DISCUSSION

We have seen that the particle trajectory and cloud masking analyses obtain isolation of moist convective updrafts within the troposphere, which allows us to understand how important these updrafts are to generating momentum flux, kinetic energy and other quantities within the troposphere. The updrafts account for a large percentage of the vertical component of the perturbation kinetic energy, but the largest amount of perturbation

kinetic energy is due to horizontal motions outside of the storm itself.

The comparison of the wave energy flux to the perturbation kinetic energy of the troposphere demonstrated that the vertically-propagating gravity waves generated by the convection can be interpreted as a sink for the convection.

Future research will include applying the above analyses to additional simulations of convection. In addition, we will perform lag correlations between measures of tropospheric convective activity and stratospheric wave activity.

7. ACKNOWLEDGMENTS

This research was supported in part by a grant from the National Science Foundation (ATM-9812384), and by a grant from the U.S. Department of Energy (DE-FG03-95ER62102).

8. REFERENCES

Alexander, M. J., J. R. Holton, and D. R. Durran, 1995: The gravity wave response above deep convection in a squall line simulation. *J. Atmos. Sci.*, **52,** 2212-2226.

Baldwin, M. P., L. J. Gray, T. J. Dunkerton, K. Hamilton, P. H. Haynes, W. J. Randel, J. R. Holton, M. J. Alexander, I. Hirota, T. Hironouchi, D. B. A. Jones, J. S. Kinnersley, C. Marquardt, K. Sato, and M. Takahashi, 2001: The quasi-biennial oscillation. *Rev. Geophys.* (in press).

Bretherton, F. P., 1969: Momentum transport by gravity waves. *Quart. J. Roy. Meteor. Soc*., **95,** 213-243.

Dunkerton, T. J., 1997: The role of gravity waves in the quasi-biennial oscillation. *J. Geophys. Res.*, **102,** 26,053-26,076.

Eliassen, A., and E. Palm, 1960: On the transfer of energy in stationary mountain waves. *Geofys. Publikasjoner*, **22,** No. 3, 1-23.

Fovell, R. G., D. R. Durran, and J. R. Holton, 1992: Numerical simulations of convectively generated stratospheric gravity waves. *J. Atmos. Sci.*, **49,** 1427-1442.

Fritts, D. C., and G. D. Nastrom, 1992: Sources of mesoscale variability of gravity waves. Part II: Frontal, convective, and jet stream excitation. *J. Atmos. Sci.*, **49,** 111-127.

Krueger, S. K., G. T. McLean, and Q. Fu, 1995: Numerical simulation of the stratus-to-cumulus transition in the subtropical marine boundary layer. Part II: Boundary-layer circulation. *J. Atmos. Sci.*, **52,** 2851-2868.

Pfister, L., S. Scott, M. Loewenstein, S. Bowen, and M. Legg, 1993: Mesoscale disturbances in the tropical stratosphere excited by convection: Observations and effects on the stratospheric momentum budget. *J. Atmos. Sci*, **50,** 1058-1075.

Randall, D. A., and D.-M. Pan, 1993: Implementation of the Arakawa-Schubert parameterization with a prognostic closure. *The Representation of Cumulus Convection in Numerical Models*, K. Emanuel and D. Raymond, Eds. Meteor Monogr. Vol. 24, No. 46., p. 137-144.

Weisman, M. L., and J. B. Klemp, 1982: The dependence of numerically simulated convective storms on vertical wind shear and buoyancy. *Mon. Wea. Rev.*, **110,** 504-520.

Xue, M., K. K. Droegemeier, V. Wong, 2000: The Advanced Regional Prediction System (ARPS) - A multi-scale nonhydrostatic atmospheric simulation and prediction model. Part I: Model dynamics and verification. *Meteorol. Atmos. Phys.*, **75,** 161-193.